Catal Lett (2009) 127:312–318
DOI 10.1007/s10562-008-9680-5

Effect of Calcination Temperature on Properties of Eggshell Ni/MgO–Al_2O_3 Catalyst for Partial Oxidation of Methane to Syngas

Yejun Qiu · Jixiang Chen · Jiyan Zhang

Received: 4 July 2008 / Accepted: 16 September 2008 / Published online: 7 October 2008

Abstract The effect of calcination temperature on the properties of eggshell Ni/MgO–Al_2O_3 catalysts was studied. Catalyst deactivation was also investigated. It is found that higher calcination temperature contributes to lower surface area, wider pore, and larger Ni crystallites. Small Ni crystallites and large pores favor the catalyst performance. Catalyst deactivation is due to the formation of NiO–MgO solid solution and/or $NiAl_2O_4$, phase transformation, and sintering.

Keywords Nickel catalyst · Eggshell catalyst · Partial oxidation of methane · Syngas · Calcination temperature

1 Introduction

Partial oxidation of methane (POM) to syngas has been one of the most attractive and challenging tasks since 1990. This reaction is a mild exothermic process and produces syngas with H_2/CO ratio of 2:1, and it overcomes some drawbacks of methane steam reforming and CO_2 reforming reactions, such as high cost.

Nickel-based catalysts, especially $A1_2O_3$ supported nickel catalysts, have received much attention for POM reaction because of their lower cost and similar activity and selectivity in comparison with noble metal catalysts [1]. However, at high temperature, the reaction between Ni species with $A1_2O_3$ results in the formation of $NiMg_2O_4$ spinel, which is difficult to be reduced and catalytically inactive for POM [2]. In addition, carbon deposition related to the acidity of $A1_2O_3$ and the sintering of metallic nickel also lower catalytic activity and lead catalyst deactivation. In order to avoid the above problems, Ni/$A1_2O_3$ is generally promoted with alkali metals, alkaline-earth metals, and rare-earth metals oxides. Among these, MgO is widely used [3–7]. Choudhary et al. [3] have reported that the MgO precoated Ni/Al_2O_3 catalyst shows much better performance than the one without precoating. This is mainly due to the formation of stable $NiMg_2O_4$ spinel protective layer and so the elimination or drastic reduction in the formation of $NiA1_2O_4$ spinel. Due to the formation of $NiMg_2O_4$ spinel, the sintering of the catalyst and the nickel crystallites can be restrained [4, 5]. As a basic promoter, MgO also favors decreasing coke deposition through eliminating acidic sites and promoting CO_2 adsorption [5, 7]. Recently, we have prepared the MgO promoted eggshell Ni/Al_2O_3 catalyst, which also exhibited better performance than eggshell Ni/Al_2O_3 catalysts [8]. Because POM is a very fast reaction and can fulfill in a few milliseconds inside a small volume catalytic bed [9, 10], the inner diffusion affects strongly the catalytic performance for the Ni/Al_2O_3 catalysts with a diameter of about 1.5 mm [11]. This is the reason for better performance of the eggshell Ni/Al_2O_3 catalyst which has higher effective factor. To our knowledge, few researchers have investigated the performance of nickel-based catalysts with large particles in POM reaction. We suggest that the nickel-based catalysts with eggshell distribution show a promising application for POM.

Y. Qiu · J. Chen (✉) · J. Zhang
Department of Catalysis Science and Engineering, School of Chemical Engineering and Technology, Tianjin University, Tianjin 300072, China
e-mail: jxchen@tju.edu.cn

Y. Qiu
Department of Material Science and Engineering, Harbin Institute of Technology, Shenzhen Graduate School, Shenzhen 518055, China

It is well known that the catalyst performance is closely related to the preparation methods and conditions [6, 12, 13], such as calcination temperature. In the present work, in order to modify the performance of eggshell Ni/MgO–Al_2O_3 catalyst, the effect of calcination temperature on its properties was investigated by means of N_2 adsorption, H_2-TPR, XRD, and TGA. The catalyst stability was tested, and the reasons for the catalyst deactivation were also investigated.

2 Experimental

2.1 Catalyst Preparation

γ-Al_2O_3 spheres with 1.5 mm diameter were provided by Shandong Aluminum Company of China. They were pre-calcined at 823 and 1,273 K for 4 h, respectively, and were then impregnated with $Mg(NO_3)_2$ aqueous solution. Afterward, the spheres were calcined at 723 K for 2 h. Thus, two MgO modified Al_2O_3 supports, labeled as MgO–Al_2O_3, were obtained. S-1273 and S-823 denote the MgO–Al_2O_3 supports, in which γ-Al_2O_3 was pre-calcined at 1,273 and 823 K, respectively.

The two prepared supports were impregnated with the aqueous solution of $Ni(NO_3)_2$ for 3 min, dried under 433 K and 101 kPa conditions for 2 h, and then calcined at 383, 823, and 1273 K for 4 h, respectively. Five catalysts were prepared, and labeled as Ni(383)/S-1273, Ni(823)/S-1273, Ni(383)/S-823, Ni(823)/S-823, and Ni(1273)/S-823, where the number in the parentheses denotes the calcination temperature of the catalyst. The Ni content in all catalysts is about 10 wt.%.

2.2 Catalyst Characterization

Specific surface area was measured by N_2 adsorption method at 77 K on a Micromeritics ASAP 2020 instrument. Prior to measurement, the sample was outgassed at 573 K under nitrogen flow for 4 h. The Brunauer-Emmett-Teller (BET) equation was used to calculate the specific surface area, S_{BET}. X-ray powder diffraction (XRD) patterns were obtained on a PANalytical's X'Pert PRO diffractometer with Co-Kα radiation operated at 40 kV and 40 mA. The crystallite phase was determined by the data of JCPDS. The average size of nickel crystallites was estimated from XRD line-broadening method by employing Scherrer equation. The line distribution profile of Ni element in the cross section of spherical catalyst was measured by an Oxford ISIS-300 energy-dispersion X-ray spectroscopy (EDX). In this measurement, the catalyst particles were split into two parts along a certain axis so as to expose the cross section. H_2 temperature programmed reduction (H_2-TPR) was carried out in a U-tube quartz reactor. The reduction was conducted in a 10 vol% H_2/N_2 flow (40 mL min^{-1}) at a heating rate of 15 K/min. The signal of hydrogen consumption was detected using a thermal conduction detector (TCD). Thermogravimetric Analysis (TGA) was carried out on a Pyris Diamond TG instrument. The air flow was 100 mL min^{-1}, and the heating rate was 15 K/min.

2.3 Catalyst Reactivity Tests

Catalyst reactivity tests were carried out in an atmospheric continuous flow fixed-bed quartz reactor (i.d. = 5 mm). In order to decrease the difference in temperature and avoid channeling or bypassing that could occur when the large catalyst spheres (>0.5 mm) were used in the small diameter reactor, the catalyst spheres were mixed with quartz powder (0.15–0.25 mm in diameter). The catalyst was firstly reduced in situ in a 10 vol% H_2/N_2 flow at 1,073 K for 30 min. After the reduction, the temperature of the catalyst bed decreased to the designated one, and a feed mixture with a CH_4/O_2 molar ratio of 2:1 was introduced into the reactor. The gaseous products were analyzed with an online chromatograph equipped with a TCD and a TDX-101 packed column.

3 Results and Discussion

3.1 Textural Properties of Catalysts

Table 1 lists the S_{BET} and average pore diameters of the supports and the catalysts. Support S-1273 has lower S_{BET} and larger pore diameter than S-823 because it was calcined at higher temperature. The high temperature calcination leads the transformation of γ-Al_2O_3 to α-Al_2O_3, and so the decrease of S_{BET} and the increase of the pore size [14]. As a result, under the same preparation conditions, the S-1273 supported nickel catalysts have lower S_{BET} and larger pore size than S-823 supported ones. The fact that Ni(823)/S-1273 has higher S_{BET} than Ni(383)/S-1273 is attributed to the complete decomposition of $Ni(NO_3)_2$. However, the S_{BET} values of Ni(383)/S-823, Ni(823)/S-823, and Ni(1273)/S-823 are 3.2, 72.2 and 46.9 m^2/g, respectively. For the S-823 supported catalysts, when the calcination temperature is lower than 823 K, the sintering of γ-Al_2O_3 is negligible and the decomposition of $Ni(NO_3)_2$ is important for affecting the pore structure of the catalysts. Higher temperature makes more amount of $Ni(NO_3)_2$ be decomposed, which results in the less blockage of pores with $Ni(NO_3)_2$. When the calcination temperature is higher than 823 K, $Ni(NO_3)_2$ decomposes fully and the sintering of γ-Al_2O_3 becomes more important, which leads the decrease of the S_{BET}. This is why S_{BET}

Table 1 Specific surface areas and average pore diameters of support and catalyst samples

Catalyst sample	Specific surface area (cm^2/g)	Average pore diameter (nm)
S-1273	49.0	16.5
S-823	97.5	6.3
Ni(383)/S-1273	0.6	3.8
Ni(823)/S-1273	30.6	16.3
Ni(383)/S-823	3.2	3.4
Ni(823)/S-823	72.2	5.8
Ni(1273)/S-823	46.9	16.1

increases first and then decreases for the S-823 supported catalysts when the calcination temperature increases from 383 to 1,273 K.

Table 1 also shows that the pore size increases with the increase of calcination temperature for S-1273 and S-823 supported catalysts. The increasing calcination temperature favors the decomposition of $Ni(NO_3)_2$ and the sintering of the catalysts, both of which benefit the increase of the pore size.

3.2 XRD Results

Figure 1 presents the XRD patterns of the catalysts reduced at 1,073 K for 30 min. The XRD patterns of S-1273 supported catalysts show more diffraction peaks than those of S-823 supported ones. This is attributed to the phase transformation of γ-Al_2O_3 to κ-Al_2O_3, θ-Al_2O_3, and α-Al_2O_3 due to S-1273 calcined at 1,273 K. No κ-Al_2O_3, θ-Al_2O_3, and α-Al_2O_3 form in the S-823 supported catalysts. Even if Ni(1273)/S-823 was prepared via calcination at 1,273 K, no phase transformation of γ-Al_2O_3 occurred due to the modification of MgO. The phase transformation of γ-Al_2O_3 is related to the condensation of the hydroxyl groups and the existence of the cation defects. The condensation of the hydroxyl groups into water leads to Al–O–Al bridges. It has been hypothesized that mobile species (AlOH) are responsible for sintering [15–17]. MgO modification can decrease or eliminate the mobile species and the defects through the formation of $MgAl_2O_4$ spinel, which inhibits the phase transformation of γ-Al_2O_3 and the formation of $NiAl_2O_4$ as well.

As shown in Fig. 1, there are the diffraction peaks located at $2\theta = 44.5°$, 52.0°, and 76.4° attributed to metallic Ni. Based on the crystal face of Ni(200), the nickel crystallite sizes for Ni(383)/S-823, Ni(823)/S-823, and Ni(1273)/S-823 are about 8.3, 13.0, and 27.2 nm, respectively. It is difficult to calculate the nickel crystallite sizes in Ni(383)/S-1273 and Ni(823)/S-1273 because of the overlapping of the diffraction peaks of α-Al_2O_3 and Ni^0 at $2\theta = 52.5°$. However, the diffraction peaks of Ni^0 in

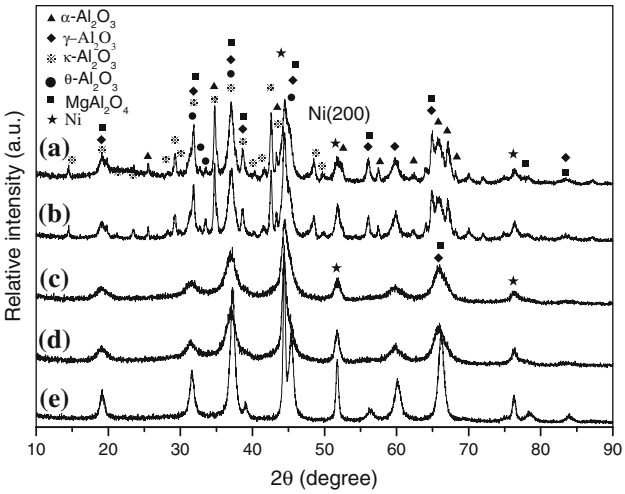

Fig. 1 XRD patterns of catalyst samples reduced at 1,073 K. a Ni(383)/S-1273; b Ni(823)/S-1273; c Ni(383)/S-823; d Ni(823)/S-823; e Ni(1273)/S-823

Ni(823)/S-1273 are sharper than those in Ni(383)/S-1273, indicating that Ni(823)/S-1273 has larger metallic Ni crystallites. It is clear that the sintering of the nickel crystallites occurs with increasing calcination temperature, similar to the result of the Ref. [18].

3.3 Nickel Distribution: Optical Photos and EDX Results

The optical photos and nickel line distribution profile of the cross section for the reduced Ni(383)/S-1273 are shown in Fig. 2. Remarkably, nickel element mainly distributes in the surface layer of Ni(383)/S1-1273, i.e., shows an eggshell-type distribution. The average thickness of the eggshell is about 0.2 mm.

3.4 H_2-TPR Results

Figure 3 shows the H_2-TPR profiles of the different catalysts. There is a remarkable peak at about 630 K in the profiles of Ni(383)/S-823 and Ni(383)/S-1273, which can be related to the decomposition of $Ni(NO_3)_2$.

In the profile of Ni(1273)/S-823(Fig. 3e), only one peak at about 1,180 K is attributed to the reduction of $NiAl_2O_4$ spinel [19]. There is no same peak for Ni(383)/S-823 and Ni(823)/S-823 (Fig. 3b, d), indicating that $NiAl_2O_4$ does not form. This is related to the low calcination temperatures. In comparison to Ni(383)/S-823, there is a more obvious peak at 980 K and no peak at 790 K in the profile of Ni(823)/S-823. This is attributed to higher temperature calcination for Ni(823)/S-823, which leads stronger interaction between Ni species and the support.

In the TPR profiles of Ni(383)/S-1273 and Ni(823)/S-1273, a reduction peak centers at 1062 and 1083 K,

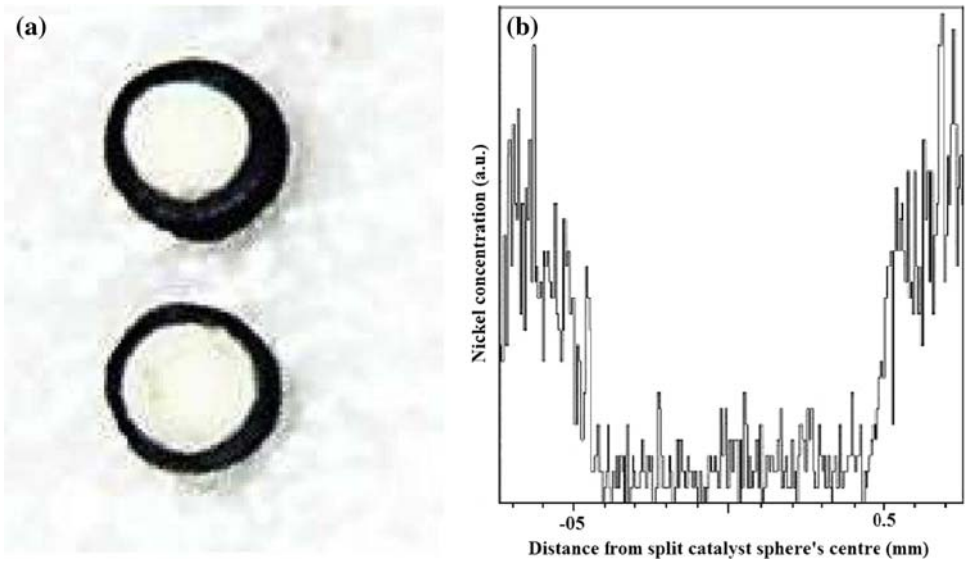

Fig. 2 Optical photos and nickel line distribution profile of cross section of reduced Ni(383)/S-1273 (Ni Kα) by EDX analysis

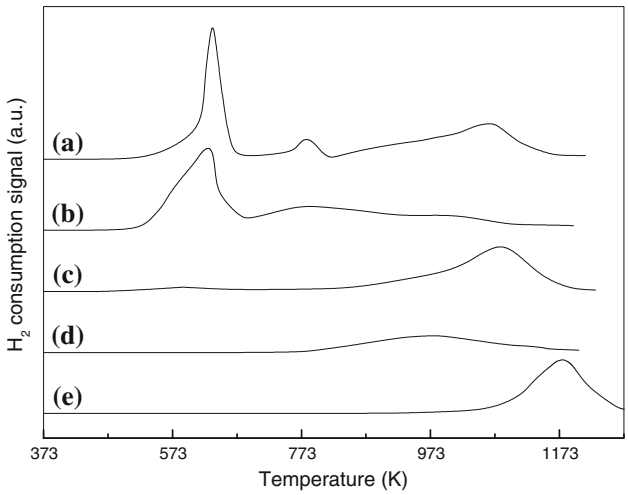

Fig. 3 H_2-TPR profiles of different catalyst samples (**a**) Ni(383)/S-1273; (**b**) Ni(383)/S-823; (**c**) Ni(823)/S-1273; (**d**) Ni(823)/S-823; (**e**) Ni(1273)/S-823

respectively, which probably is attributed to the reduction of Ni species in NiO–MgO solid solution [20]. Calcined at 1,273 K, γ-Al_2O_3 is transformed into κ-Al_2O_3, θ-Al_2O_3, and α-Al_2O_3 phases to some degree (as shown in Fig. 1). The formation of κ-Al_2O_3, θ-Al_2O_3 and α-Al_2O_3 can decrease the interaction between MgO and Al_2O_3, and MgO is prone to react with NiO to form NiO–MgO solid solution, in which nickel species are difficult to be reduced.

3.5 Catalyst Activity and Selectivity

Figure 4 shows the performance of the different catalysts in POM reaction. For the catalysts prepared under the same conditions, the S-1273 supported catalysts show better catalytic performance than the S-823 supported ones. For example, at the temperature of 773 K, the CH_4 conversions over Ni(383)/S-1273 and Ni(823)/S-1273 are 9.1% and 10.4% higher than those of Ni(383)/S-823 and Ni(823)/S-823, respectively. In this work, Ni(383)/S-1273 shows the best activity. At the temperature of 1073 K and the space velocity of 8×10^4 h^{-1}, the CH_4 conversion, CO and H_2 selectivities over Ni(383)/S-1273 reach 97.5%, 94.3%, and 94.3%, respectively.

POM is a very fast reaction [6]. The inner diffusion is very important for the catalysts with the diameter of about 1.5 mm, and so the eggshell catalysts show better catalytic performance [8]. Besides the nickel distribution, the pore structure of the catalysts also affects the catalyst activity. S-1273 supported Ni catalysts have larger pore diameter (Table 1), which is favorable to the diffusion of CH_4 and O_2 molecules, and they show higher catalytic activities than S-823 supported catalysts. Ni(383)/S-1273 exhibits better activity than Ni(823)/S-1273 although the former has smaller pore diameter (Table 1). The unreduced Ni(383)/S-1273 catalyst has small pore size due to the blockage by undecomposed $Ni(NO_3)_2$, however, $Ni(NO_3)_2$ can decompose during the reduction, so the reduced Ni(383)/S-1273 and Ni(823)/S-1273 possibly have similar pore structure. On the other hand, the reduced Ni(383)/S-1273 have smaller nickel crystallites (Fig. 1), which can promote the catalyst activity. Ni(383)/S-823 and Ni(823)/S-823 show lower activity, which is related to their smaller pore size. It is worthy to note that the activity of Ni (1273)/S-823 is superior to that of Ni (823)/S-1273. Ni (1273)/S-823 and Ni (823)/S-1273 have the similar diameters, while the nickel crystallites in Ni (1273)/S-823 catalyst are larger than those of Ni (823)/S-1273 (as shown in Fig. 1). This result can be attributed to the following reasons. As analyzed in the Sect. 3.4, the interaction between MgO and NiO in Ni (1273)/S-823 is less than that in Ni (823)/S-1273. In other words, the reduced metal nickel is easer to

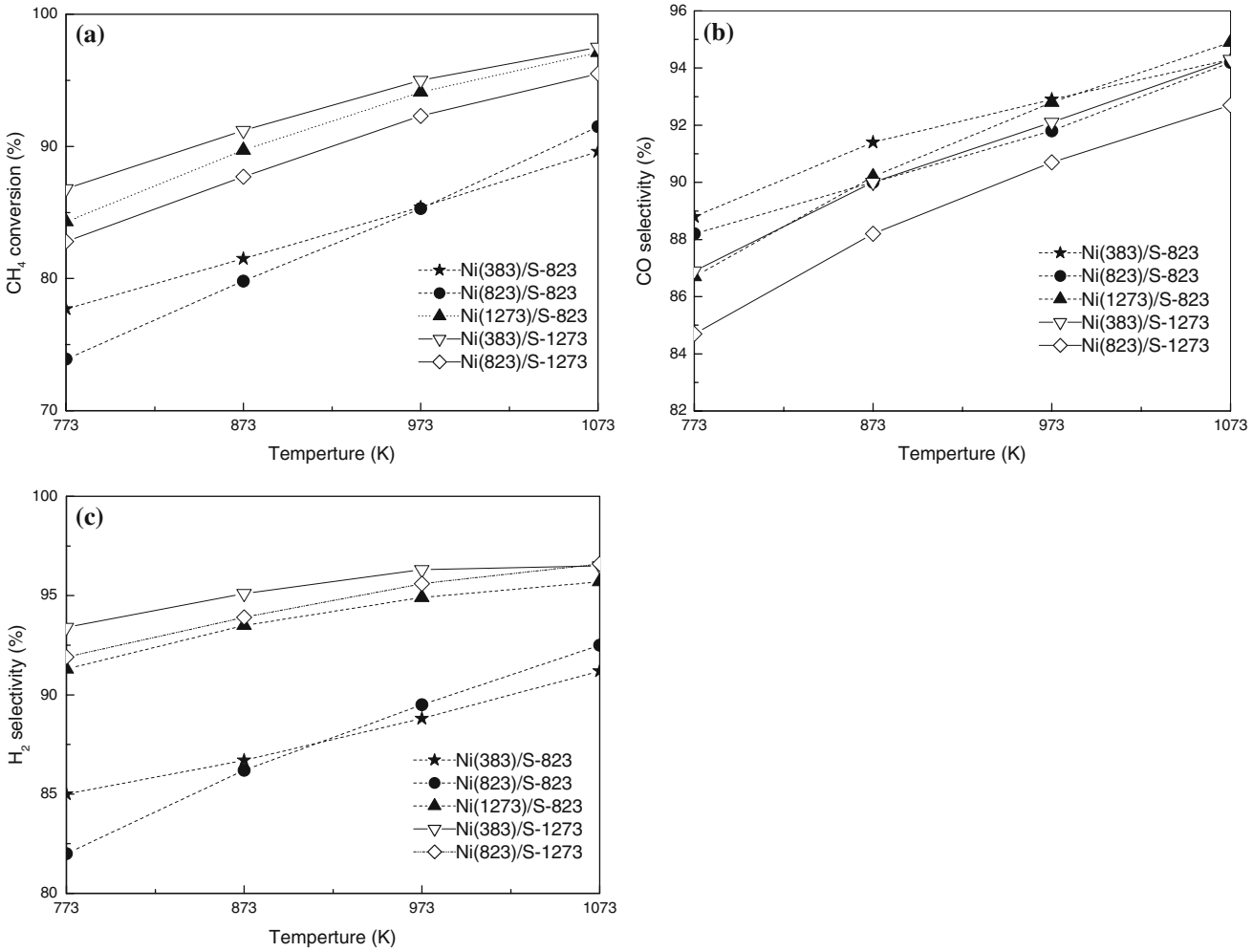

Fig. 4 Reactivities of different catalysts in POM reaction **a** CH_4 conversion; **b** CO selectivity; **c** H_2 selectivity. Reaction conditions: 0.1 MPa, 0.1 g catalyst, CH_4:O_2 = 2:1, GHSV = 8×10^4 h^{-1}

react with MgO in Ni (823)/S-1273 in the POM system that is of oxidative and reductive synchronously. The formation of the solid solution can decrease the amount of the metallic Ni that is essentially responsible to the activity [21]. In addition, Ni (1273)/S-823 has larger S_{BET} than Ni (823)/S-1273.

3.6 Catalyst Stability and Deactivation

3.6.1 Catalyst Stability

Ni(383)/S-1273 catalyst shows high initial activity in POM reaction. It is very significant to test its stability further. Figure 5 shows the stability of Ni(383)/S-1273 during 100 h. In the first 20 h, CH_4 conversion, CO and H_2 selectivities maintain constant. Nevertheless, after 20 h, they begin to decrease. After reaction for 100 h, in comparison to the initial ones, CH_4 conversion, CO and H_2 selectivities decrease about 3.0%, 1.3%, and 1.2%, respectively. In addition, the used catalyst is greatly different from the fresh one in color. The fresh Ni(383)/S-1273 is black due to Ni^0, However, the used Ni(383)/S-1273 at the different position in the catalyst bed has different color: the top part is green, the middle part is sage green, and the bottom one is black. This indicates that the chemical valence of nickel distributes from +2 to 0 from the top to the bottom in the used catalyst.

3.6.2 Analysis of Catalyst Deactivation

Dissanayake et al. [22] have pointed out that coke is an important reason for the catalyst deactivation in POM reaction. In the present work, thermogravimetric analysis (TGA) technique was adopted to measure the carbon deposition on the Ni(383)/S-1273 used for 100 h, and the result is presented in Fig. 6. The TG curve can be classified into three stages: the first is the weight loss stage from room temperature to 500 K, resulting from the evaporation

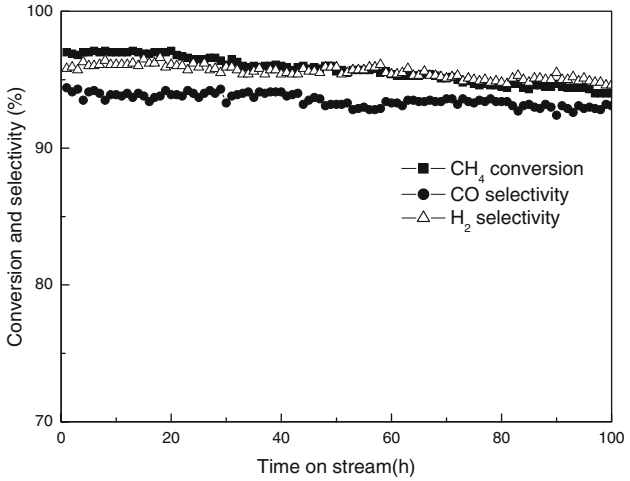

Fig. 5 Performance of Ni(383)/S-1273 with time on stream in POM reaction. Reaction conditions: 0.1 g catalyst, 1073 K, 0.1 MPa, CH_4:O_2 = 2:1, GHSV = 8×10^4 h^{-1}

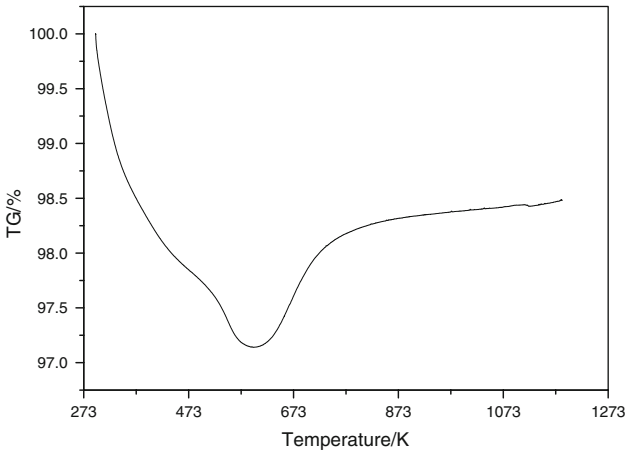

Fig. 6 TG curve of Ni(383)/S-1273 used for 100 h

of adsorbed water; the second is the weight loss stage from 500 to 570 K, attributing to the oxidation of carbon; the last is weight gain stage from 570 to 800 K, originating from the oxidation of Ni^0. The surface carbonaceous species generated by methane decomposition can be classified into three types: C_α, C_β and C_γ [23]. C_α is corresponding to carbide and can be hydrogenated at temperatures below 323 K, and C_β is amorphous carbon and hydrogenable between 373 and 573 K [24]. C_α and C_β are the intermediate species to form syngas and can not lead to the catalyst deactivation. C_γ is graphitic carbon with poor activity, which can cover the active sites and result in the catalyst deactivation. The carbon in Ni(383)/S-1273 can be eliminated between 500 and 570 K, and this temperature range is far below the reaction temperature. Moreover, the coke amount is very less (about 0.6 wt.%). Thus, the carbon deposition is not the important reason for the deactivation of Ni(383)/S-1273.

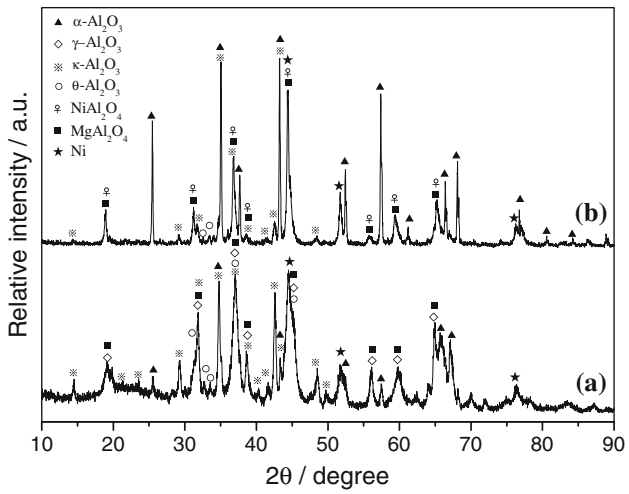

Fig. 7 XRD patterns of a fresh and b used Ni(383)/S-1273

Another possible reason leading to the deactivation of nickel-based catalysts in POM is the phase transformation of Al_2O_3 [2]. Figure 7 shows the XRD pattern of Ni(383)/S-1273 after reaction for 100 h. In comparison to the XRD pattern of the fresh Ni(383)/S-1273, the diffraction peaks due to α-Al_2O_3 in the used Ni(383)/S-1273 become sharper, indicating that α-Al_2O_3 crystallites become larger. Meanwhile, the diffraction peaks attributed to γ-Al_2O_3, κ-Al_2O_3 and θ-Al_2O_3 become weaker or disappear, indicting that γ-Al_2O_3, κ-Al_2O_3 and θ-Al_2O_3 transform into more stable α-Al_2O_3 phase. Thus, the phase transformation of Al_2O_3 is a reason for the deactivation of Ni(383)/S-1273. Additionally, the diffraction peaks due to Ni^0 located at $2\theta = 44.5°$, 52.0°, and 76.4° become sharper in used Ni(383)/S-1273 than the fresh one. The sintering of the metallic Ni crystallites is another reason for the catalyst deactivation.

Figure 8 provides the H_2-TPR profile of the used Ni(383)/S-1273. In the profile, there are four reduction

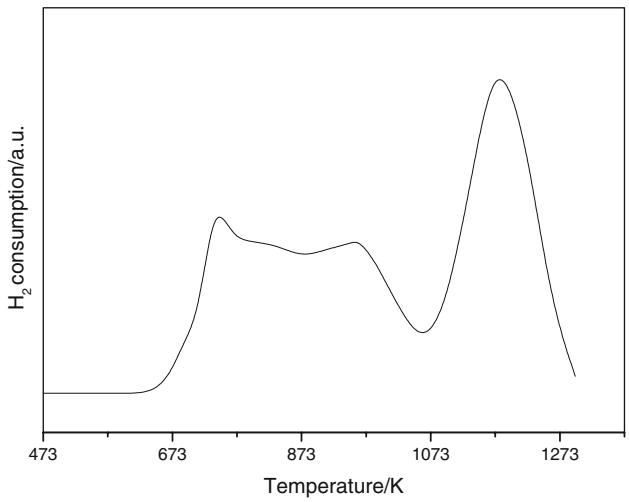

Fig. 8 H_2-TPR profile of Ni(383)/S-1273 after reaction for 100 h

peaks at about 750, 790, 960 and 1180 K, respectively. The former three peaks are attributed to the reduction of surface NiO species with different interaction between NiO and support. The last reduction peak is attributed to the reduction of NiO–MgO solid solution or $NiAl_2O_4$ spinel, and this peak area occupies about 1/2 in the whole reduction peak area. The Ni species in NiO–MgO solid solution and $NiAl_2O_4$ spinel are difficult to be reduced and thus can not participate in the POM reaction, which is probably the main reason to cause the deactivation of Ni(383)/S-1273.

4 Conclusion

Due to the phase transformation and the sintering of γ-Al_2O_3, support S-1273 has lower specific surface area and larger pore diameter than support S-823. The textural properties of the supports make an important influence on the catalyst performance. The calcination temperature also influences the physicochemical properties of Ni/MgO–Al_2O_3 catalysts. Lower calcination temperature results in better reducibility and smaller nickel crystallites. The important factors influencing the catalyst performance are the nickel crystallite size and the pore diameter of the catalyst. Small nickel crystallites and large pores are favorable to improve the catalyst performance.

Ni(383)/S-1273 possesses good activity and selectivity in POM reaction. During the life test, it was very stable in the first 20 h and deactivated slightly after 100 h. The important reasons for the catalyst deactivation include the formation of NiO–MgO solid solution and/or $NiAl_2O_4$ spinel, the phase transformation, and the sintering.

References

1. Ashcroft AT, Cheetham AK, Foord JS, Green MLH, Grey CP, Murrell AJ, Vernon PDF (1990) Nature 344:319
2. Zhang YH, Xiong GX, Sheng SS, Yang WS (2000) Catal Today 63:517
3. Choudhary VR, Uphade BS, Mamman AS (1995) Catal Lett 32:387
4. Qiu YJ, Chen JX, Zhang JY (2007) Front Chem Eng China 1:167
5. Requies J, Cabrero MA, Barrio VL, Cambra JF, Güemez MB, Arias PL, Parola VL, Peña MA, Fierro JLG (2006) Catal Today 116:304
6. Koo KY, Roh HS, Seo YT, Seo DJ, Yoon WL, Park SB (2008) Int J Hydrogen Energy 33:2036
7. Koo KY, Roh HS, YTc Seo, Seo DJ, Yoon WL, Park SB (2008) Appl Catal A 340:183
8. Qiu YJ, Chen JX, Zhang JY React Kinet Catal Lett (accepted for publication)
9. Hickman DH, Schimdt LD (1992) J Catal 138:267
10. Choudary VR, Mamman AS, Sansare SD (1992) Angew Chem Int Ed Engl 31:1189
11. Qiu YJ, Chen JX, Zhang JY (2007) Catal Commun 8:508
12. Song YQ, He DH, Xu BQ (2008) Appl Catal A 337:19
13. Utaka T, Al-Drees SA, Ueda J, Iwasa Y, Takeguchi T, Kikuchi R, Eguchi K (2003) Appl Catal A 247:125
14. Andryushkova OV, Kirichenko OA, Ushakov VA, Poluboyarov VA (1997) Solid State Ion 101–103:647
15. Johnson MFL (1990) J Catal 123:245
16. Burtin P, Brunelle JP, Pijolat M, Soustelle M (1987) Appl Catal 34:225
17. Burtin P, Brunelle JP, Pijolat M, Soustelle M (1987) Appl Catal 34:239
18. Sehested J, Gelten JAP, Remediakis IN, Bengaard H, Nørskov JK (2004) J Catal 223:432
19. Schulze K, Makowski W, Chyży R, Dziembaj R, Geismar G (2001) Appl Clay Sci 18:59
20. Nurunnabi M, Mukainakano Y, Kado S, Miyazawa T, Okumura K, Miyao T, Naito S, Suzuki K, Fujimoto KI, Kunimori K, Tomishige K (2006) Appl Catal A 308:1
21. Wang SB, Lu GQM (1998) Appl Catal B 16:269
22. Dissanayake D, Rosynek MO, Kharras KCC, Lunsford JH (1991) J Catal 132:117
23. Zhang ZL, Verykios XE (1994) Catal Today 21:589
24. Chen L, Lua Y, Hong Q, Lin J, Dautzenberg FM (2005) Appl Catal A 292:295